Imaging using volume holograms

Arnab Sinha
George Barbastathis
Massachusetts Institute of Technology
Department of Mechanical Engineering
Room 3-466
77 Massachusetts Avenue
Cambridge, Massachusetts 02139
E-mail: arnab@mit.edu

Wenhai Liu
Ondax Incorporated
850 East Duarte Road
Monrovia, California 91016

Demetri Psaltis, FELLOW SPIE
California Institute of Technology
Department of Electrical Engineering
1200 East California Boulevard
MS 136-93
Pasadena, California 91125

Abstract. We present an overview of imaging systems that incorporate a volume hologram as one of the optical field processing elements in the system. We refer to these systems as volume holographic imaging (VHI) systems. The volume hologram is recorded just once, and the recording parameters depend on the functional requirements of the imaging system. The recording step offers great flexibility in designing application-specific imaging systems. We discuss how a VHI system can be configured for diverse imaging applications ranging from surface profilometry to real-time hyperspectral microscopy, and summarize recent developments in this field. [DOI: 10.1117/1.1775230]

Subject terms: imaging systems; volume holography.

Paper VHOE-B02 received Dec. 10, 2003; revised manuscript received Jan. 29, 2004; accepted for publication Feb. 27, 2004.

1 Introduction

Traditional optical imaging systems, such as photographic cameras, microscopes, telescopes, and projection lenses are composed of an optical train, i.e., several lenses in succession. The role of the lenses is to transform the optical field such that the resulting field distribution at the image plane meets the functional requirements of the system. For example, in traditional photographic imaging the goal is to create a projection of a 3-D field onto a 2-D receptor plane (photosensitive film or digital sampling plane). Within the constraints of projective geometry, the 2-D image is intended to be geometrically similar to the original 3-D object. The dependence of the selection of the optical train on the goal of the instrument can be seen by comparing a microscope and a telescope. In the microscope, one aims for lateral magnification from an object plane at a finite distance, whereas in the telescope the object is at infinity and the goal is angular magnification.[1] So the two systems are very different in the way they transform ray bundles (or equivalently, spatial frequencies).

Nevertheless, traditional optical systems are very similar with respect to certain other features. Most prominent among these features is defocus, which is directly related to depth information (that is, the third spatial dimension). In classical optics, a defocused object creates a blurred image, independent of the type of optics used (even though the blur transfer function is of course highly dependent on the specific choice of optics). Information about the third dimension is lost in the process, but it can be partially recovered with digital postprocessing even from a single camera image, for example depth from defocus,[2] depth from shading,[3,4] etc., or from multiple cameras.[5] The confocal microscope[6] is exceptional because the confocal pinhole almost eliminates out-of-focus light at the expense of field of view. Other optical instruments, such as coherence imagers in the space domain[7–10] and time domain,[11] laser radar,[12] and Radon transform tomographers[13] acquire depth information via different mechanisms and tradeoffs.

We describe a new type of optical element, a volume holographic lens.[14] The volume holographic lens is a prerecorded volume hologram[15] that is incorporated into the optical train in addition to the other traditional lenses that are already present in the train. The traditional refractive lenses perform simple 2-D processing operations on the optical field[16] as it passes through the optical train and is incident on the volume holographic lens. The volume holographic lens processes the optical field in 3-D on account of its thickness,[17] i.e., it has Bragg selectivity.[18] The field diffracted by the volume holographic lens is measured to obtain the specific information that is required about the optical field.

The volume holographic lens is manufactured by recording a 3-D interference pattern of two (or more) mutually coherent beams, as shown in Fig. 1(a). The recording is independent of the object to be imaged, although the selection of the type of hologram to be recorded (e.g., the type of reference beam) can be based on prior information about the type of objects to be imaged (e.g., the average working distance, reflective versus fluorescent, etc.). Simple recording schemes include interfering a spherical reference (SR) or planar reference (PR) beam with a planar signal beam to record holograms (see Fig. 2) in the transmission, reflection, or 90-deg geometry.[14] After recording is complete, the hologram is fixed;[19,20] no further processing is done on the hologram (just like the fixed lenses in an imaging instrument after they are ground and polished). Despite the apparent simplicity of recording, these holograms offer unique imaging capabilities that are not available in traditional lenses.

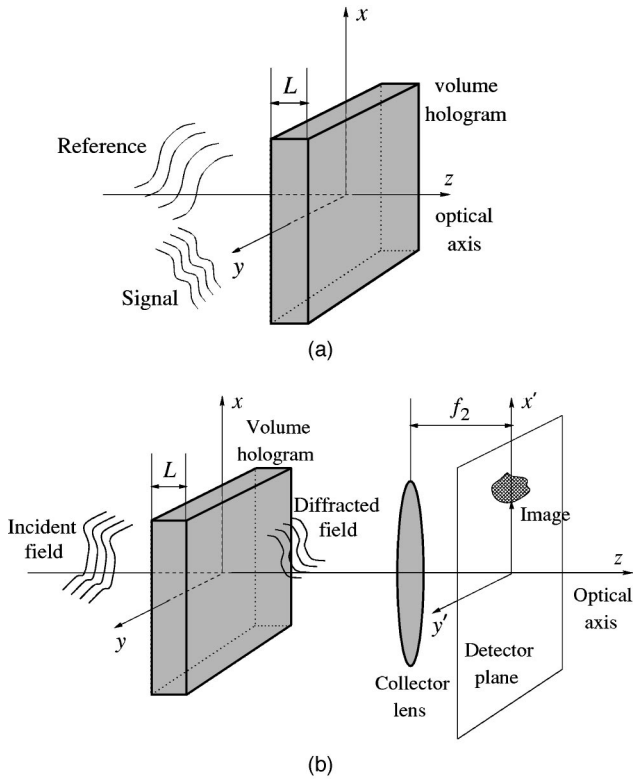

Fig. 1 General schematic of volume holographic imaging. (a) The volume grating is the recorded 3-D interference pattern of two mutually coherent beams. (b) The imaging step consists of reading out the volume hologram by an unknown object illumination. The volume hologram diffracts only the Bragg-matched components of the object illumination. This effect is used in conjunction with scanning to recover the object illumination.

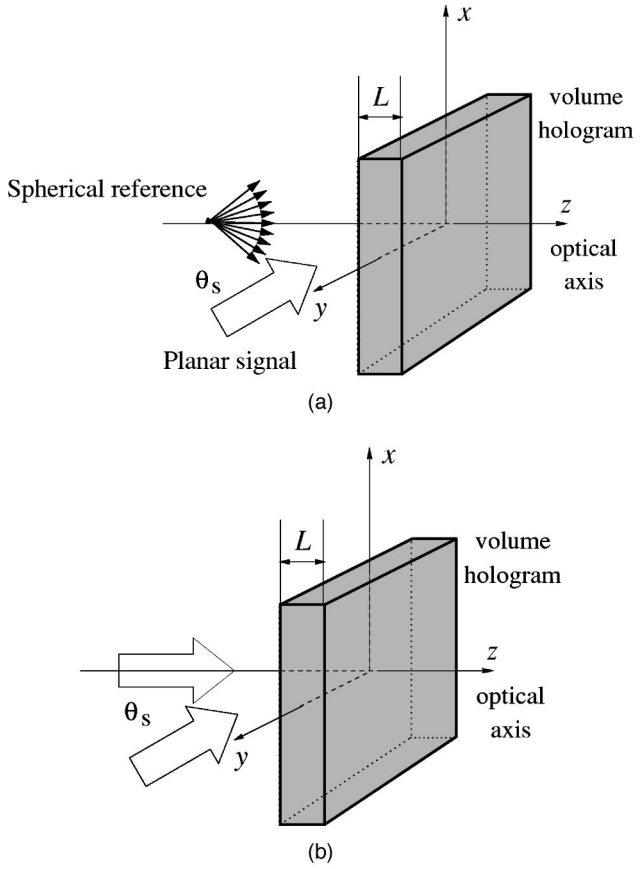

Fig. 2 Simple volume holographic recording schematics: (a) spherical reference (SR) hologram and (b) planar reference (PR) hologram. Note that both schematics are transmission holograms. Other recording geometries can also be used.

During imaging, the recorded holograms are probed by the incident illumination, as shown in Fig. 1(b). If an SR hologram is used, the imaging system is referred to as SR-VHI. Similarly, a PR-VHI system refers to a system that contains a planar reference volume hologram. The hologram diffracts the Bragg-matched[17,18] components of the incident illumination. The diffracted field is monitored by a detector or a detector array. The diffracted field intensity captured by the detector is the ''image'' formed by the VHI system, and can be used to determine the required object information like the 3-D spatial and/or spectral characteristics of the object of interest.

This work is arranged as follows. In Sec. 2, we describe various classes of imaging systems with particular emphasis on their VHI implementations. In Sec. 3, we present various VHI systems that we have demonstrated and discuss each in detail. Finally, we conclude in Sec. 4 with some directions for future work in VHI.

2 Classification of VHI Systems

2.1 *Type of Object/Illumination*

The material properties of the object and the type of illumination determine the nature of the image as follows.

1. Reflective surfaces are opaque. A system imaging a reflective surface typically returns an image of the form $\{z(x,y),r(x,y)\}$. The function r specifies the reflectivity of the surface as a function of the lateral coordinates (x,y). The function $z(x,y)$ is referred to as the surface ''profile'' of the object, and the imaging instrument is called a surface profilometer.
2. 3-D point scatterers consist of a several small point sources distributed over a volume. A system imaging this object returns an image $I(x,y,z)$, where the function I specifies the scattering strength at object location (x,y,z). Fluorescent particles suspended within a fluid are a good example of this kind of object.
3. A 3-D translucent/absorptive object has some refractive index and absorption variation within the object volume. A system imaging this object would return an image $n(x,y,z)+i\alpha(x,y,z)$, where n refers to the refractive index and α the absorption coefficient at object location (x,y,z). Tomographic imaging systems like computed tomography (CT) are used to image 3-D absorptive objects.

Further, the nature of the illumination used for imaging can be classified as follows. 1. Active illumination relies on external sources to pump light to the object. The imaging system collects the reflected/backscattered light for imag-

ing. 2. Passive illumination schemes rely on either self-luminescence or ambient light to provide the necessary illumination for imaging.

VHI can be implemented for all of these classes of objects and illumination, as we discuss later in Sec. 3.

2.2 *Single Hologram/Many Multiplexed Holograms*

The Bragg selectivity property of volume diffraction allows several gratings to be multiplexed inside the same volume of the photosensitive material.[18] This means that a VHI system can comprise: 1. one single volume holographic grating that acts as a lens for imaging, or 2. several gratings, i.e., several lenses multiplexed[21] within the same volume element. Each of these gratings can independently process the optical information; this reduces both the back-end digital computation and the scanning time required. However, there is a tradeoff involved, since the diffraction efficiency decreases[22] as the number of multiplexed gratings increase.

We discuss both schemes later in Sec. 3.

2.3 *Single/Multiple VHI Sensors in the Imaging System*

The resolution of VHI, like most other imaging systems, degrades[23] with increasing object distance. Often, traditional lens-based imaging systems use triangulation methods to accurately determine depth information about objects, even though each sensor by itself can image only in 2-D. In triangulation,[5] several sensors image the same object from different directions. The different images are combined geometrically to yield a high-resolution profile of the object. A similar approach can be used for VHI to offset the degradation of depth resolution by using multiple VHI sensors to acquire different perspectives of the object of interest and improve image resolution by reconciling these perspectives into one consolidated image. Thus, a VHI system could comprise: 1. a single VHI sensor to acquire the object information on its own, or 2. multiple VHI sensors to acquire multiple perspectives of the same object. The perspectives can be reconciled using various numerical techniques such as point multiplication of the individual point spread functions (PSFs), least-squares error optimization, or an expectation maximization algorithm. We refer to this setup as *N*-ocular VHI.

We discuss both single and *N*-ocular VHI schemes in Sec. 3.

2.4 *Type of Objective Optical System*

A volume hologram is very sensitive to the incident illumination and diffracts only the Bragg-matched components of the illumination. Often, it is possible to manipulate the illumination to Bragg match the hologram at different object distances by using specific objective optical systems, for instance, microscope objective optics placed in front of the volume hologram can configure the VHI system to image objects at short working distances with very high resolutions, and telescope and telephoto objective optics placed in front of the hologram can configure the VHI system to image objects at long working distances also with high resolution.

We discuss both microscope and telescope schemes in Sec. 3.

3 VHI Implementations

Volume holograms possess Bragg selectivity, which helps a VHI system to optically segment[14] the object space and selectively identify special attributes (for instance spatial locations, spectral signatures, etc.) of interest. We have previously[24] derived the impulse response as a function of axial defocus for both SR- and PR-VHI systems. Figure 3(a) is a schematic of a SR-VHI system. The diffracted field intensity as a function of the detector coordinates is calculated under the first Born approximation to be

$$\frac{I(x',y';\delta)}{I_b(\theta_s f_2,0;\delta)} = \left| \mathcal{L}\left\{ \frac{2\pi a^2 \delta}{\lambda d^2}, \frac{2\pi a}{\lambda f_2}[(x'-\theta_s f_2)^2 + y'^2]^{1/2} \right\} \times \mathrm{sinc}\left\{ \frac{[x'^2 + y'^2 - (\theta_s f_2)^2]L}{2\lambda f_2^2} \right\} \right|^2. \quad (1)$$

In Eq. (1), (x',y') are the detector coordinates, λ is the wavelength of light used, δ is the longitudinal defocus from the Bragg-matched longitudinal location d, $\theta_s \ll 1$ rad is the inclination of the planar signal beam, L is the thickness of the hologram, a is the radius of the hologram aperture, and $I_b(\theta_s E,0;\delta)$ is the diffraction intensity at the Bragg-matched detector coordinates. $\mathcal{L}(\cdot,\cdot)$ is a function that represents the intensity distribution near the focus of a lens. Figure 3(b) shows an experimentally obtained diffracted field for a SR-VHI system to verify the theory.

Figure 4(a) is a schematic of a PR-VHI system. The diffracted field intensity in this case is derived as in Ref. 24 and,

$$\frac{I(x',y';\delta)}{I_b(\theta_s f_2,0;\delta)} = \mathrm{circ}\left\{ \frac{[(x'-\theta_s f_2)^2 + y'^2]^{1/2}}{f_2 a\,\delta / f_1^2} \right\} \times \mathrm{sinc}^2\left[\frac{L\theta_s}{\lambda}\left(\frac{x'}{f_2} - \theta_s \right) \right]. \quad (2)$$

In Eq. (2), f_1 is the focal length of the collimating objective lens and δ is the longitudinal displacement from the focal point. All other parameters are the same as those of Eq. (1). Figure 4(b) shows the experimentally obtained diffracted field for a PR-VHI system. Volume holographic applications with configurations similar to SR-VHI and PR-VHI have been previously used in nonimaging contexts such as optical correlators[25] and associative memories.[26]

The depth resolution can be calculated from the impulse response by integrating over the diffracted field for different values of the defocus δ. This results in the longitudinal PSF; we define the full width at half maximum (FWHM) of the PSF as the depth resolution of the system. From Ref. 24,

$$\Delta z_{\mathrm{FWHM}}(\mathrm{SR\text{-}VHI}) = \frac{18.2 d^2 \lambda}{a^2 \theta_s L}, \quad (3)$$

and

$$\Delta z_{\mathrm{FWHM}}(\mathrm{PR\text{-}VHI}) = \frac{5.34 d^2 \lambda}{a\,\theta_s L}. \quad (4)$$

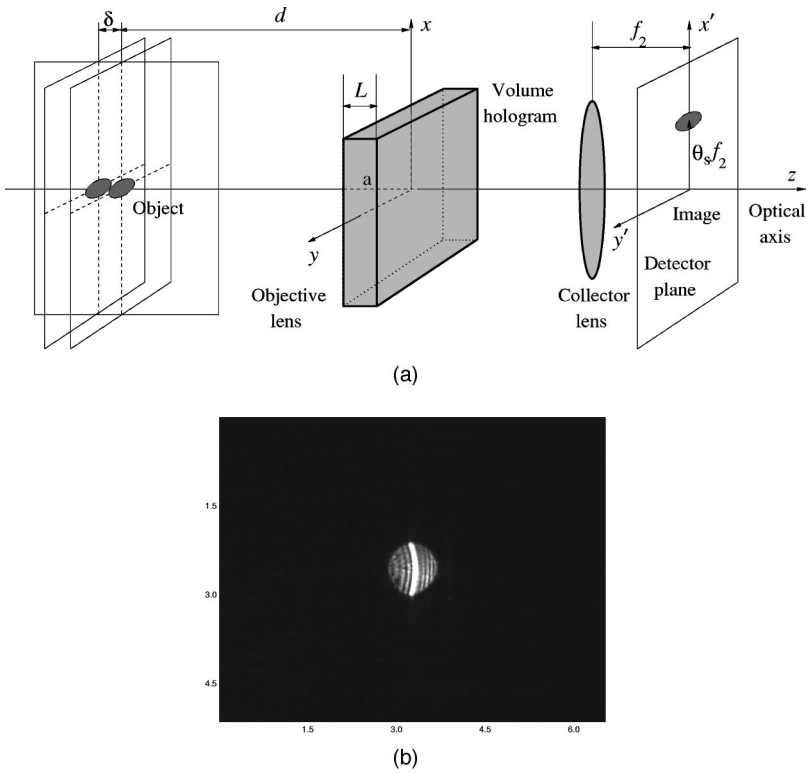

Fig. 3 (a) Schematic for transmission geometry SR-VHI. (b) Experimentally observed diffracted field, the bright strip inside the disk represents the Bragg-matched portion of the object visible to the SR hologram. Note that the strip is curved on account of the curved fringes that constitute the SR hologram. All dimensions are in millimeters unless otherwise noted.

In Eq. (4), $d=f_1$ is the working distance of the PR-VHI imaging system, all other parameters have already been defined. From Eqs. (3) and (4), we see that the depth resolution degrades quadratically with increasing object distance, similar to most imaging systems. This degradation can be offset to some extent by either making the hologram thicker (thus improving its Bragg selectivity) or increasing θ_s (this also makes the hologram more Bragg selective by reducing the grating period). We notice that Δz_{FWHM}(SR-VHI) depends on $1/a^2$, whereas Δz_{FWHM}(PR-VHI) depends only on $1/a$. This means that the constant 18.2 in Eq. (3) is unitless, but the constant 5.34 in Eq. (4) has dimensions of length. The difference between Eqs. (3) and (4) is because the SR-VHI system images objects in the Fresnel diffraction regime, whereas the PR-VHI system images objects in the Fraunhofer (on account of the collimating lens) diffraction regime.[24] This leads to interesting problems while designing the appropriate objective optics for the VHI system, and we have shown that the inverse linear dependence on aperture size of PR-VHI can be exploited to achieve optimal depth resolution at a particular working distance.[24]

VHI systems in several of the subcategories mentioned in Sec. 2 have been designed based on the simple SR and PR-VHI models. We present a brief overview and working principle for each implementation.

3.1 *Reflective Object+Active Illumination, Single Hologram, Single Sensor, No Objective Optics*

Figure 5 is the setup for stand-alone VHI without any objective optics. The single-volume hologram is recorded using a spherical reference and planar reference beam that is inclined at an angle θ_s with respect to the optical axis. The origin of the spherical reference is the Bragg-matched location for the SR-VHI system. The impulse response of the SR-VHI system is known,[24] and the resolution has been verified experimentally.[24,27]

The surface profile is recovered as follows. A laser beam is focused on the object surface and the SR-VHI system captures the reflected light. If the focused spot lies exactly on the object surface, the SR hologram is Bragg matched and a strong diffracted signal is measured. On the other hand, if the focused spot does not coincide with the object surface, the volume hologram is Bragg mismatched and the diffracted signal is much weaker. The entire object surface is recovered by scanning completely in 3-D by moving the focused spot. Figure 6 shows the experimentally obtained surface reconstruction[24] of an artifact consisting of the letters MIT that was located at a distance of $d=5$ cm from the volume hologram. The depth resolution of the system was $\Delta z_{\mathrm{FWHM}} \approx 1$ mm.

3.2 *Reflective Object+Active Illumination, Single Hologram, Single Sensor, Microscope Objective Optics*

Figure 7 shows the schematic for VHI with microscope objective optics. A single PR-volume hologram is used. The imaging is done by focusing laser light on the surface of reflective object. The light reflected by the object surface is collected by a microscope objective lens placed in front of

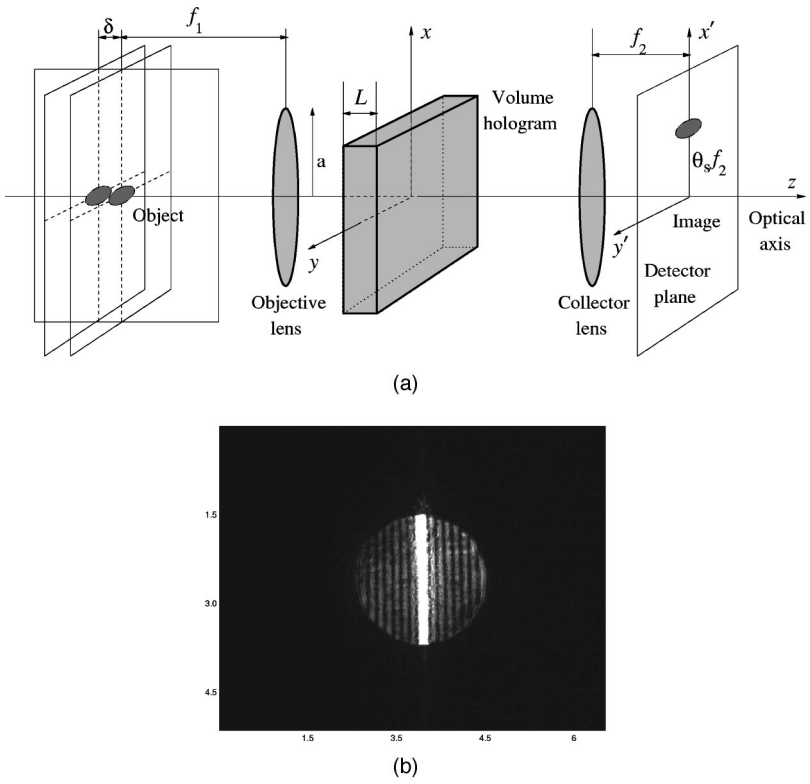

Fig. 4 (a) Schematic for transmission geometry PR-VHI. (b) Experimentally observed PR-VHI diffracted field. The straight bright slit represents the Bragg-matched slit of the object.

the hologram. If the focused spot on the surface lies at the front focal point of the microscope lens, the light is collimated and a Bragg-matched plane wave is incident on the hologram.

The detector monitors the diffracted beam from the hologram as the object is scanned in 3-D to recover the entire surface profile. Figure 8 shows experimental results for PR-VHI with microscope objective optics. The object is an analog tunable MEMS grating. The grating was located at a working distance of $d=2$ cm from the microscope objective and the depth resolution for the system was $\Delta z_{\mathrm{FWHM}} \approx 2\ \mu$m.

3.3 *Reflective Object+Active Illumination, Single Hologram, Single Sensor, Telescope/ Telephoto Objective Optics*

Figure 9 shows the schematic for VHI with objective optics for long-range surface profilometry applications. This scheme can be implemented for both SR and PR holo-

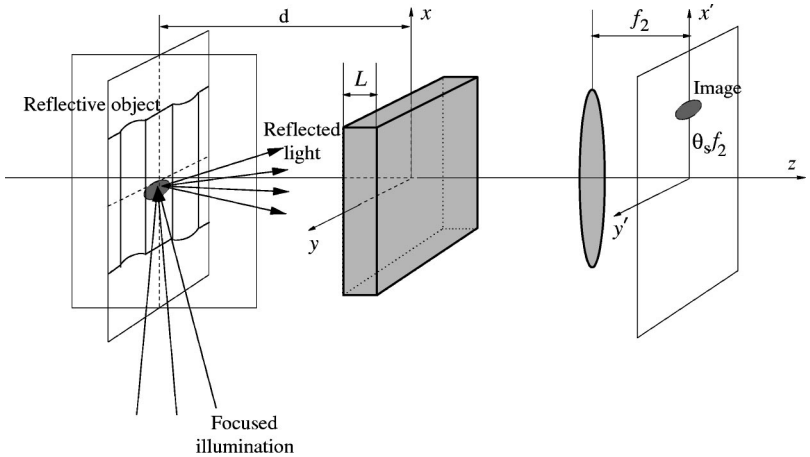

Fig. 5 VHI for reflective object+active illumination, single hologram, single sensor, no objective optics. An intensity detector monitors the beam by the SR hologram diffracted while the object is scanned in 3-D.

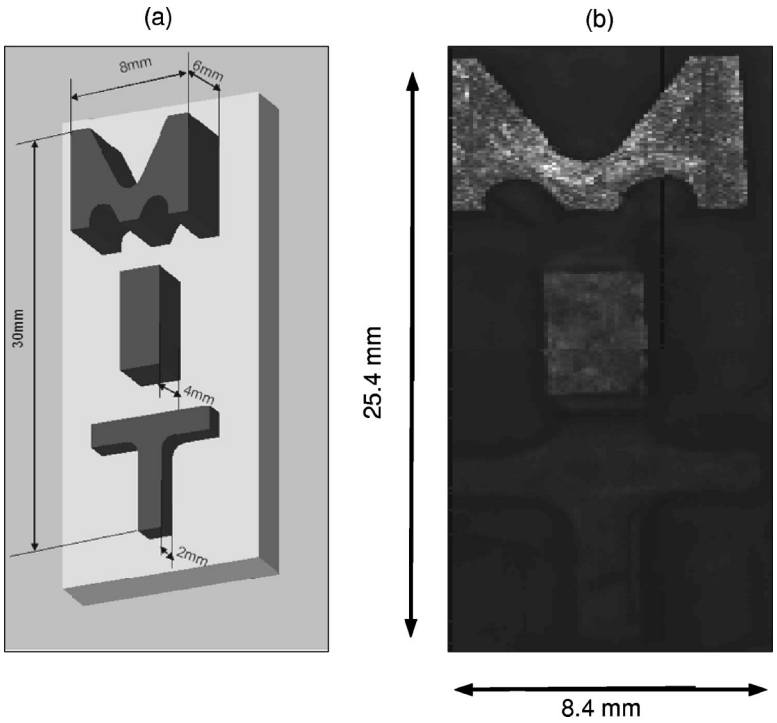

Fig. 6 Experimental VH image (from Ref. 24) of a fabricated artifact obtained using 2-mm-thick crystal of 0.03% (molar) Fe-doped $LiNbO_3$ with diffraction efficiency $\eta \approx 5\%$ recorded at $\lambda = 532$ nm. The working distance $d = 5$ cm; $a = 3.5$ mm; $\theta_s = 30$ deg; and $\Delta z_{FWHM} \approx 1$ mm. (a) is the actual CAD rendering of the object and (b) is a volume holographic image of the object obtained by a complete lateral scan with surface of the letter M being placed at the Bragg-matched location, which consequently appears to be bright.

grams. The depth resolution for most optical systems degrade quadratically with increasing object distance.[23] One way to offset this is by using optical elements with large apertures. This is expensive and impractical for volume holograms. A properly designed demagnifying telescope can have a large entrance pupil while ensuring that the field incident on the hologram placed behind the telescope is of the correct lateral extent. This permits us to increase the effective aperture of the imaging system and offset some of the degradation of depth resolution.[27]

A PR-VHI system requires collimating objective optics to Bragg match the PR hologram. In this case, a telephoto system can yield the optimal depth resolution[24] for a particular working distance. This is achieved by designing the objective optical system such that the first principal plane is as close to the object as possible. This reduces the effective

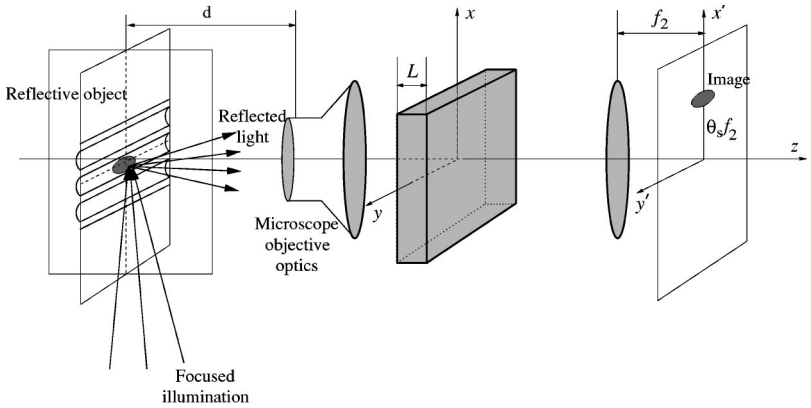

Fig. 7 VHI for reflective object+active illumination, single hologram, single sensor, microscope optics. The microscope objective collimates the light reflected from the surface and an intensity detector monitors the diffracted beam as the active probe is scanned with respect to the object.

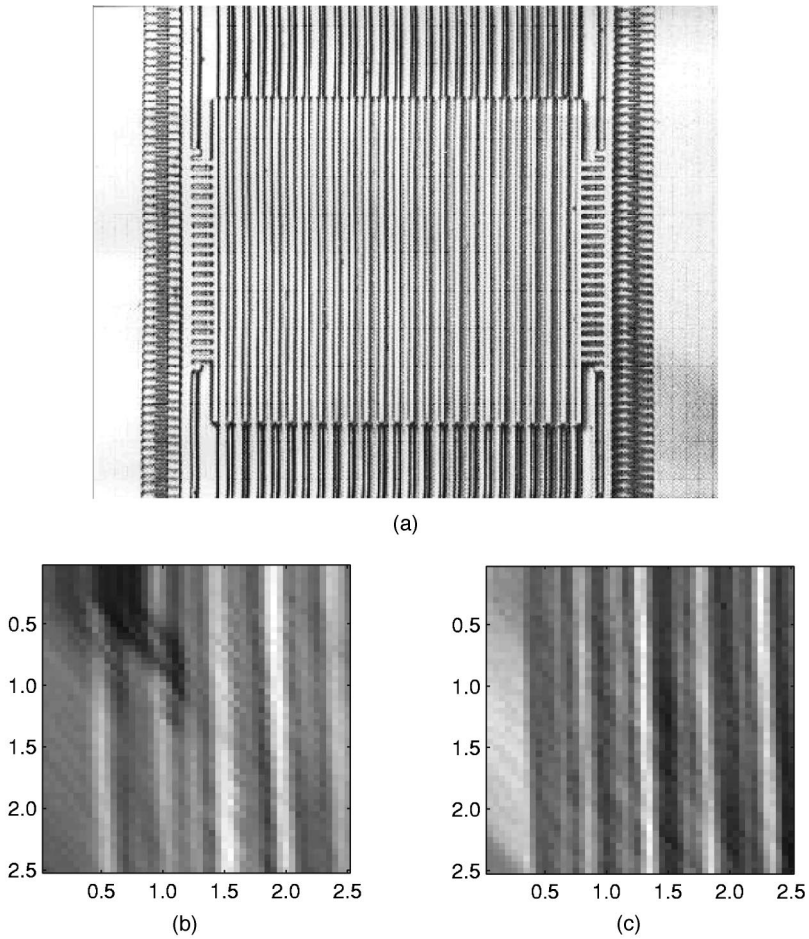

Fig. 8 VH image of a MEMS grating using microscope objective optics using the same $LiNbO_3$ crystal but recorded with a normally incident planar reference beam instead of the spherical reference. The objective optics microscope had a working distance of $d=2$ cm with $a=0.5$ cm. (a) is a picture of a MEMS grating being imaged; the height difference in between the top and bottom of the reflective grating is 24 μm. (b) VH image with laser point focused on the bottom of the grating, and (c) VH image after the focus is raised 24 μm to focus on the top of the grating surface. Note that there is a complete contrast reversal to indicate that the surfaces are indeed at different heights.

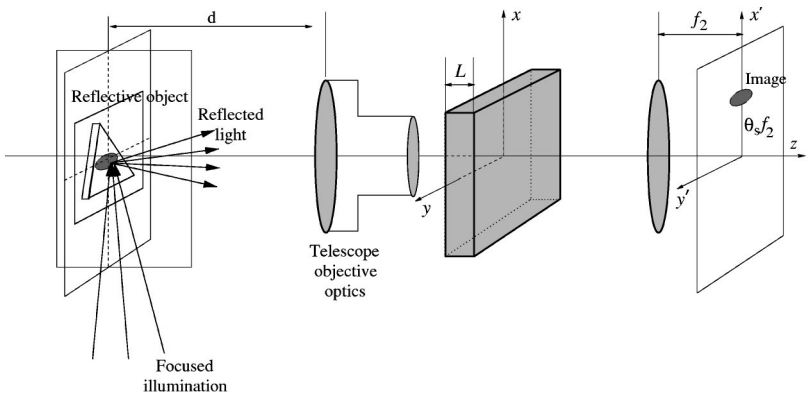

Fig. 9 VHI for reflective object+active illumination, single hologram, single sensor, telescope optics. The telescope creates a real image of the distant object in front of the SR hologram, which then diffracts according to the Bragg condition. An intensity detector monitors the diffracted beam. The entire object surface is recovered by scanning.

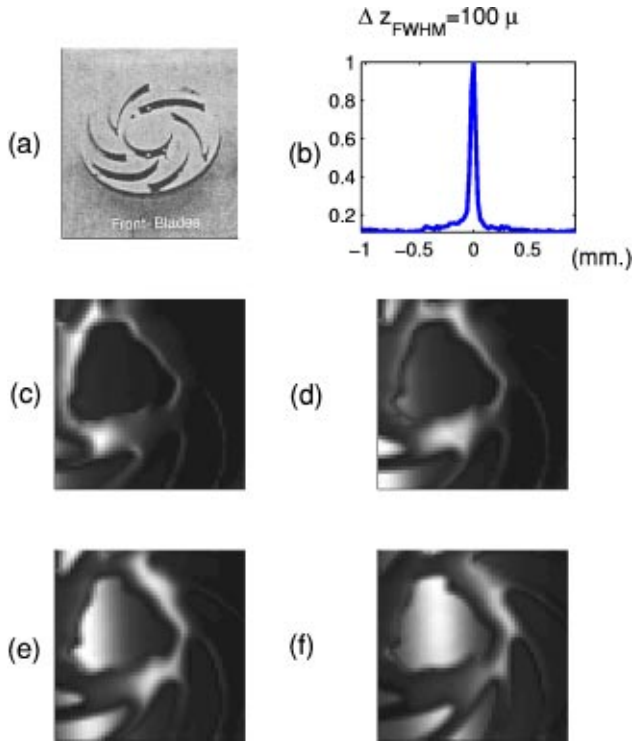

Fig. 10 VH image from Ref. 27 of a microturbine. The hologram was the same $LiNbO_3$ crystal described in Fig. 6. The telescope had angular magnification $M_\alpha = 1.5$ with $d = 16$ cm and $a = 1.2$ cm. (a) Image of the microturbine captured with a standard digital camera; the microturbine was manufactured to have surface height features of 225 μm. (b) Experimental depth response for a point source object at the same distance $\Delta z_{\mathrm{FWHM}} \approx 100\ \mu$m; (c) through (f) VH telescope scans at progressive increments of 100 μm through the object. At any given depth, the Bragg-matched portions of the object are brightest.

focal length of the system and enhances the depth resolution to the optimal diffraction-limited value.

Figure 10 shows the surface profile of a MEMS-fabricated turbine located at a working distance $d = 16$ cm away from the aperture of the objective telescope. The demagnifying telescope allowed us to resolve surface features at a resolution $\Delta z_{\mathrm{FWHM}} \approx 100\ \mu$m.

3.4 *Reflective Object+Active Illumination, Single Hologram, Single Sensor, Inclined Telephoto Objective Optics*

Figure 11 is a schematic for active VHI for reflective objects incorporating *a priori* object information to enhance depth resolution. It was noted in Sec. 3.3 that telephoto objective optics can achieve the optimal diffraction-limited depth resolution for a particular working distance when nothing is known in advance about the object. However, it is possible to incorporate *a priori* object information and enhance depth resolution even more.

For instance, consider the case when it is known that the reflective object consists of segments of flat surfaces.[28] In this case, a single PR-VHI sensor inclined with respect to the object surface can achieve substantially better depth resolution. This is possible because the *a priori* knowledge of the object surface allows us to translate the superior lateral resolution of the telephoto PR-VHI system into an apparent depth resolution by scanning the object in a direction that is inclined with respect to the object surface. Figure 12 shows the surface profile of a MEMS device, the nanogate[29] located at a working distance of $d = 46$ cm measured using an inclined PR-VHI sensor inclined at angle $\phi = 30$ deg with respect to the object surface. This sensor can resolve depth features at a resolution $\Delta z_{\mathrm{FWHM}} \approx 50\ \mu$m.

3.5 *Reflective Object+Active Illumination, Single Hologram, Multiple Sensors, Telescope Objective Optics*

The 3-D resolution of a stand-alone hologram imaging a reflective target is comparable to triangulation-based binocular imaging systems with considerable angular separation between the two cameras.[27] The resolution of VHI systems can be even further improved using multiple VHI sensors to look at the same object, as shown in Fig. 13. The two images are reconciled by point multiplying the PSF of

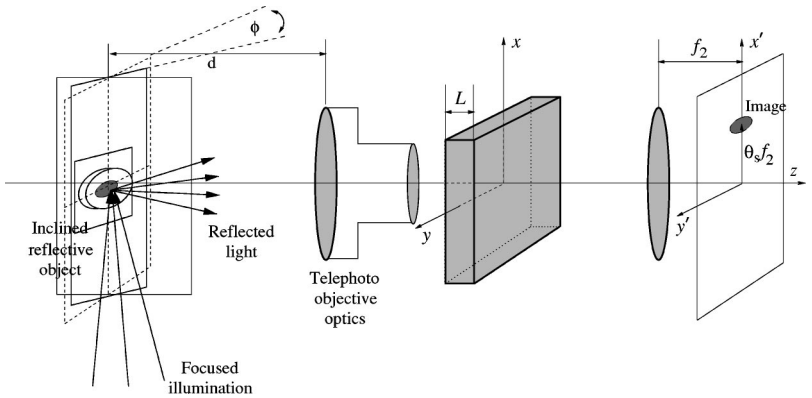

Fig. 11 VHI for reflective object+active illumination, single hologram, single sensor, inclined telephoto optics. If it is known that the object consists only of flat surfaces, depth resolution can be improved by inclining the object surface with respect to the scanning direction at an angle ϕ, as indicated. This approach exploits the superior depth resolution to improve the apparent depth resolution.

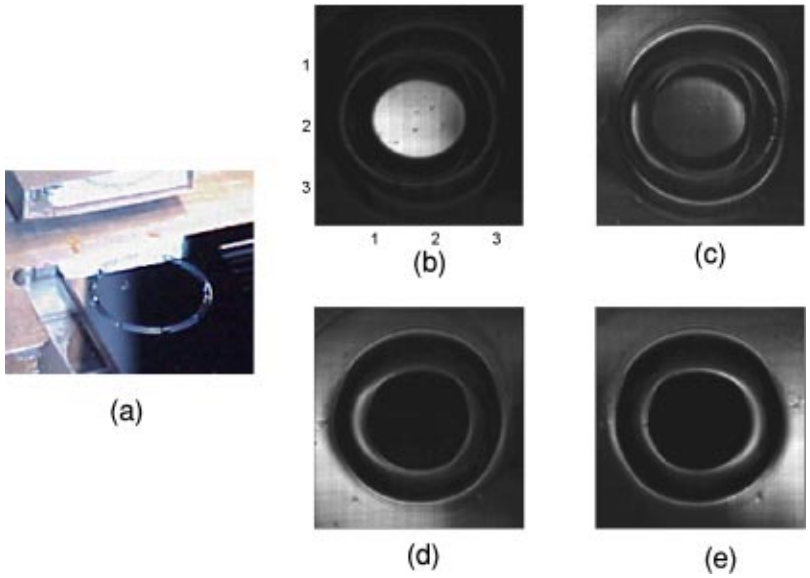

Fig. 12 From Ref. 28, a surface scan of a nanogate, which has surface features ≈150 μm using an inclined telephoto PR-VHI sensor with $d=46$ cm. (a) Image of a nanogate captured using a standard charge-coupled device (CCD). (b) PR-VHI image of device with the top surface in focus. (c) and (d) PR-VHI images focused 50 and 100 μm below the top surface. (e) PR-VHI image focused on the base of the turbine 150 μm below the top surface. Note that again there is a complete contrast reversal between images (b) and (e).

each image. The resulting image has better resolution[30] because the measurement is now overconstrained by the multiple measurements.

There are several ways to combine the multiple measurements by using digital processing, like least-squares optimization, expectation maximization, etc. The point multiplication method was implemented in the experiment of Fig. 14. Note that the point-multiplied image has better resolution than both the normal VHI and the inclined VHI sensor. However, the improvement over the inclined sensor is only marginal because the inclined sensor itself has excellent resolution. This is discussed in Sec. 3.4.

3.6 *3-D Fluorescent Object+Active Illumination, Single Hologram, Multiple Sensors, Telephoto Objective Optics*

Figure 15 is the schematic for VHI of a 3-D point-scatterer-type object. The individual sources in this case are small

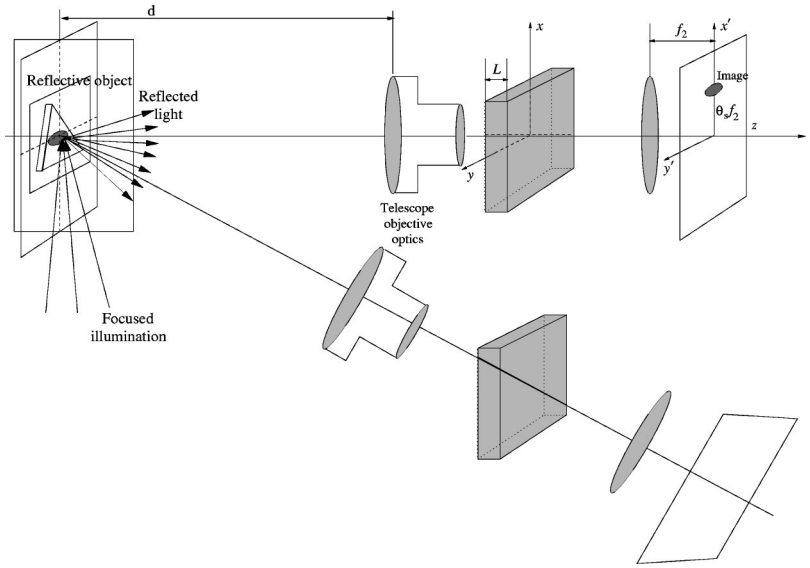

Fig. 13 VHI for reflective object+active illumination, single hologram, multiple ($N=2$) sensors, telescope optics. Multiple (we depict $N=2$) VH sensors, similar to the one described in Fig. 10, are used to simultaneously image the object. This leads to overconstraining the solution to the imaging inverse problem and results in better resolution.

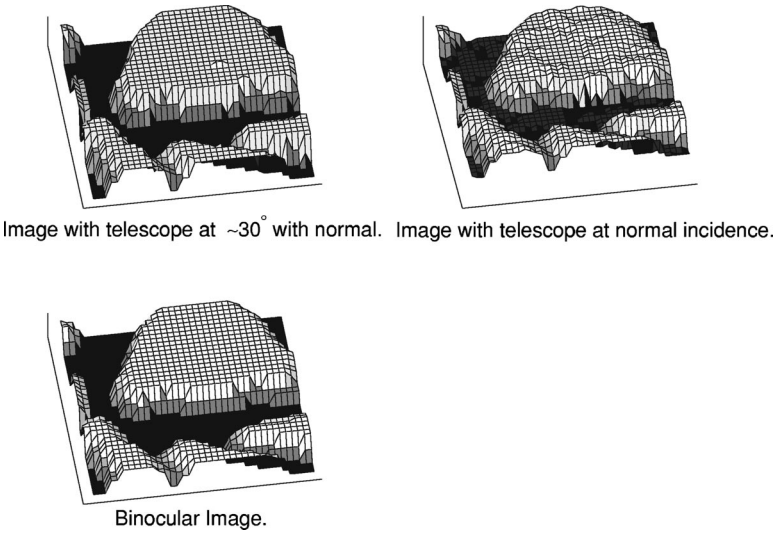

Fig. 14 Surface profiles obtained using two VHI sensors imaging the turbine described in Fig. 10. One sensor was normal to the turbine surface, the other was inclined at an angle $\phi=30$ deg with respect to the turbine surface. The resultant binocular VH image is obtained by point multiplying the individual images. Note that there is a significant improvement between the binocular and normal VHI images. However, the improvement is not as discernible between the inclined sensor and the binocular image, on account of the phenomenon described in Sec. 3.4.

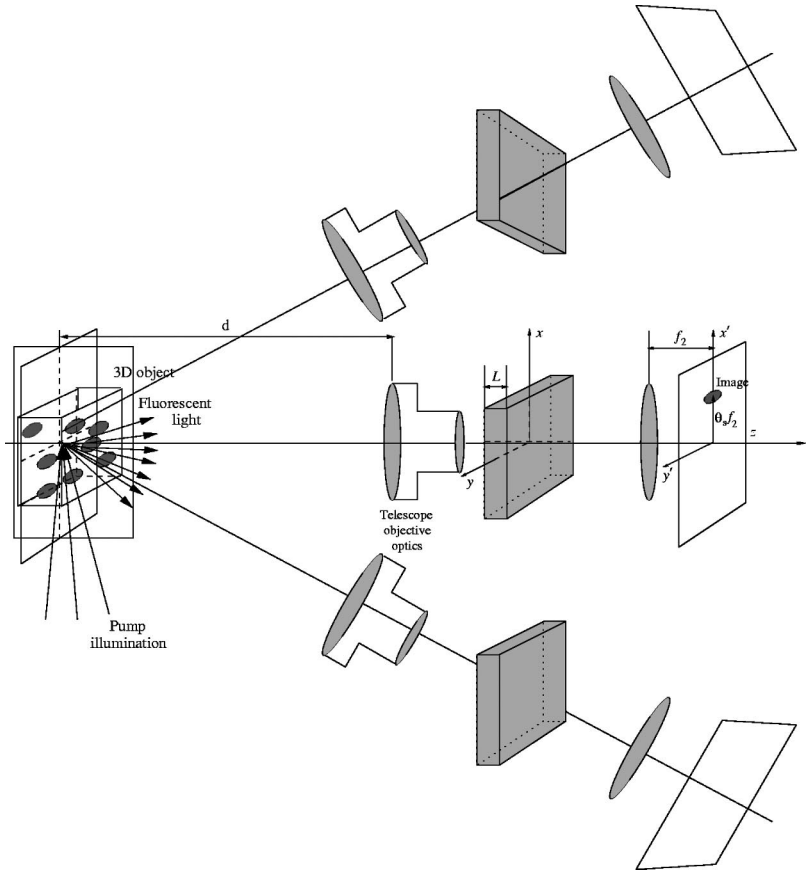

Fig. 15 VHI for 3-D fluorescent object+active illumination, single hologram, multiple ($N=3$) sensors, telephoto optics. Multiple (we depict $N=3$) VH sensors similar to that described in Fig. 12 acquire different perspectives of the fluorescent 3-D object. The multiple measurements allow for an overconstrained solution to overcome the degradation of depth resolution[32] on account of the broadband nature of the fluorescence.

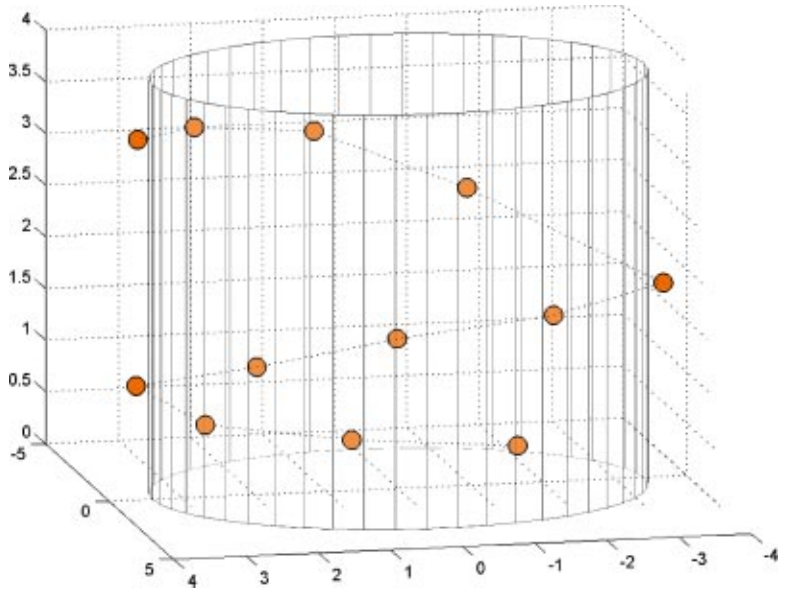

Fig. 16 3-D image of a set of fluorescent particles arranged in a helical pattern. The object was located at a working distance of $d=10$ cm from three broadband N-ocular PR-VHI sensors. The image inversion was done using pseudo-inverse techniques.[33]

beads that fluoresce on being pumped by laser illumination. Each of the three VHI sensors contains a single PR hologram with telephoto objective optics for collecting the fluorescent light. The bandwidth of the fluorescent light results in an increased field of view (FOV) with accompanying degradation of depth resolution.[31,32]

In this case, it is beneficial to reconcile the three VHI images using a least-squares optimization to obtain the actual 3-D intensity distribution of the object. The experimental results are shown in Fig. 16.[33] The 3-D object was a helical arrangement of fluorescent beads that was recovered by three VHI sensors by overconstraining the measurements using a matrix pseudo-inverse method.

3.7 *Reflective Object+Broadband Passive Illumination, Single Hologram, Single Sensor, Telephoto Objective Optics*

Figure 17 shows the schematic when a reflective object is used with a single hologram VHI sensor under conditions of broadband illumination at a long working distance. The volume hologram still has some depth resolution on account of Bragg selectivity. However, the broader the illumination bandwidth, the worse the depth resolution.[32] As a result, it is not advisable to image reflective objects using broadband VHI on account of the reduced contrast and depth resolution. This is shown in Fig. 18, which compares the contrast between surfaces for the same object as the

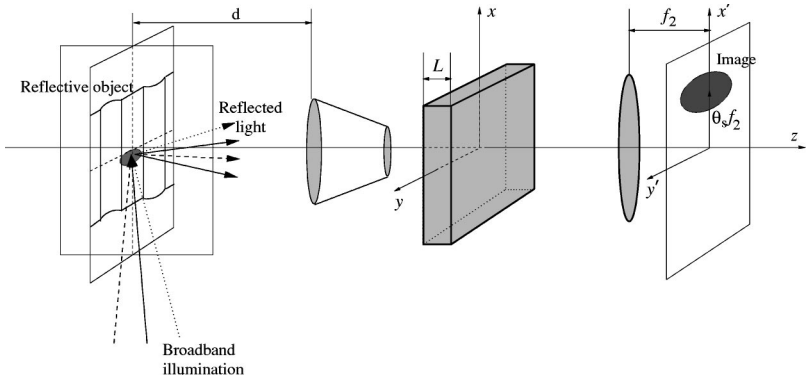

Fig. 17 VHI for reflective object+broadband (passive) illumination, single hologram, single sensor, telephoto optics. Increased illumination bandwidth improves the field of view of the VHI system, thus reducing the amount of scanning required. However, this is accompanied by degradation of the depth resolution.

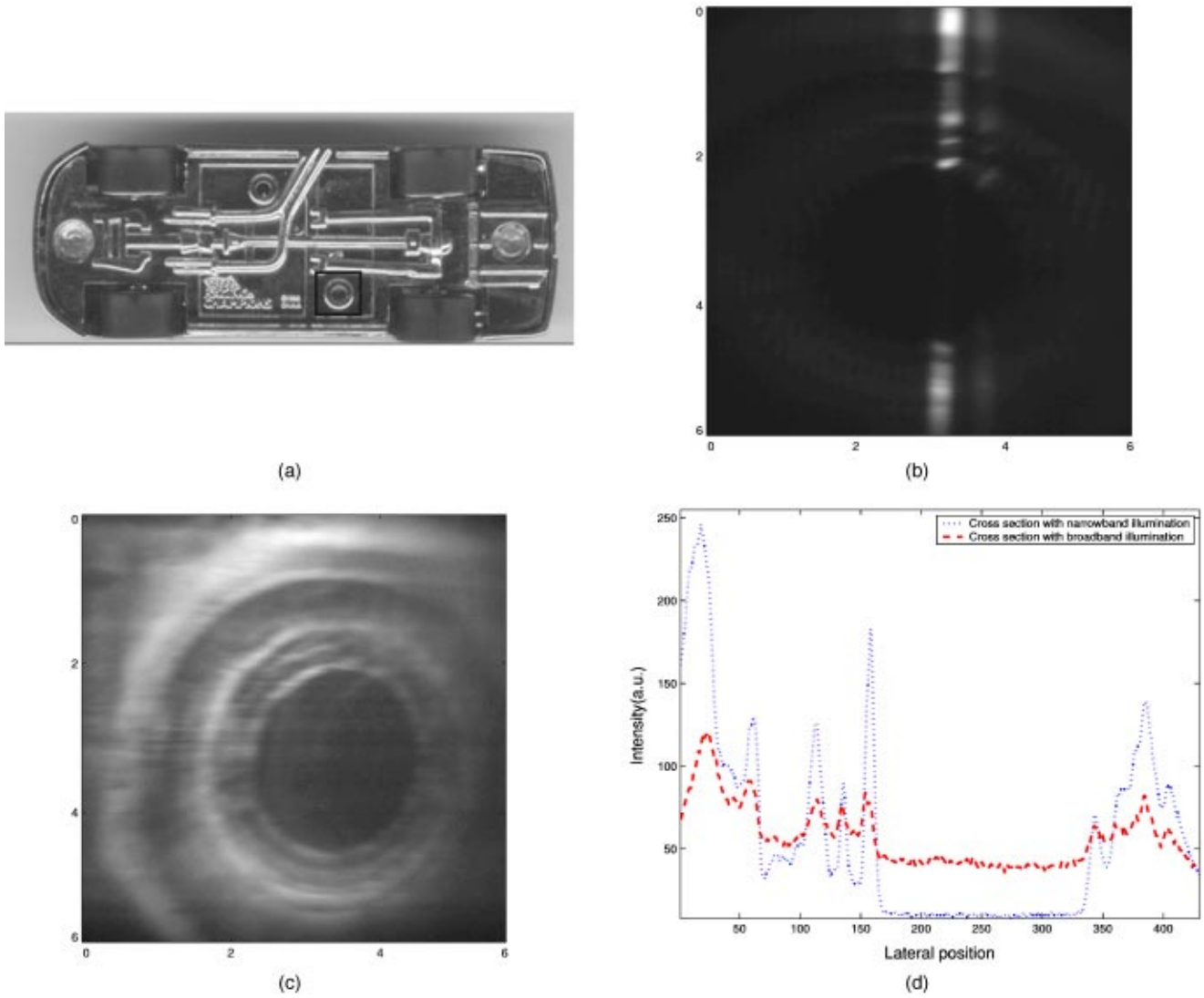

Fig. 18 From Ref. 32, surface profiles obtained using broadband illumination and PR-VHI. The object is the bottom chassis of a toy car shown in (a). The particular region of interest is a raised screw on the chassis. (b) is the VH image obtained under narrowband ($\Delta\lambda \approx 10$ nm) illumination, whereas in (c) the field of view improves under broadband ($\Delta\lambda \approx 120$ nm) illumination. However, (d) indicates that the depth resolution degrades as the illumination bandwidth increases, i.e., there is a price to pay for the enhanced field of view with respect to poorer depth discriminating ability.

illumination bandwidth is increased. The object is the bottom chassis of a toy car. Notice that the contrast between object surface features at different heights degrades as the illumination bandwidth is increased.

However, this phenomenon can be exploited to build VHI-based spectrum analyzers to measure the spectral profile of the illumination.[32]

3.8 *3-D Fluorescent Object+Active Illumination, Multiple Holograms, Single Sensor, Microscope Objective Optics*

Figure 19 is the schematic of a real-time hyperspectral microscope.[31] The object is a 3-D distribution of fluorescent beads. Three PR holograms are multiplexed inside the holographic material. Each hologram is Bragg matched at a different depth, and diffracts in a direction specified by the corresponding recording signal beam. As a result, this VHI system can simultaneously image multiple depth layers of the 3-D object. Moreover, since the fluorescent illumination is broadband, it is possible to image wide slices of each layer. The width of the slice depends on the fluorescence bandwidth. The experimental results of imaging three slices are shown in Fig. 20. To our knowledge, this is the first experimental demonstration of a real-time hyperspectral microscope in three spatial dimensions.

4 Discussion and Conclusions

We discuss several VHI implementations for a wide variety of imaging applications and demonstrate the great degree of design flexibility afforded by incorporating volume holograms in imaging systems. However, the limited diffraction of volume holograms means that some part of the object information is discarded, since we only monitor the diffracted beam in the system. An information theoretic

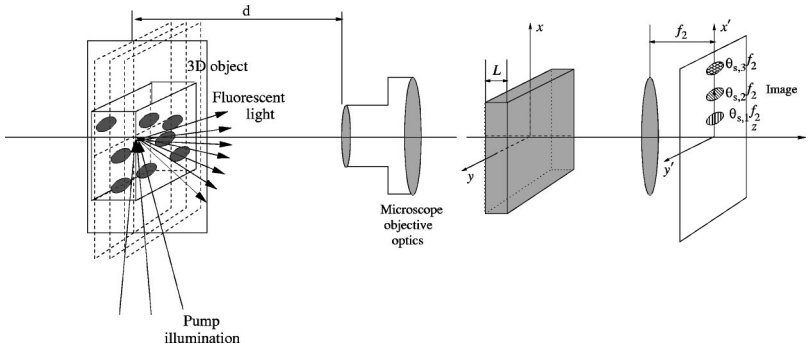

Fig. 19 VHI for 3-D fluorescent object+active illumination, multiple holograms, single sensor, microscope optics. Multiple gratings can be recorded inside the same hologram volume. This results in reduced scanning, as the VHI system can simultaneously image multiple locations within the object. This is illustrated in the figure. There are three multiplexed gratings, each observing a different depth slice of the object and then diffracting to a different location on the detector. Thus, the VHI system can simultaneously monitor three locations without any scanning.

comparison[34] between a confocal microscope with a pinhole and a confocal microscope implemented using a volume holographic filter suggests that there is a minimum diffraction efficiency required for the VHI system to outperform the nonVHI implementation. Resonant volume holography[24] is a technique that can be used to enhance the diffraction efficiency of volume holograms. It can also be used to improve the resolution in active imaging applications.

In conclusion, VHI offers great promise in designing efficient application-specific computational imaging systems where the hologram acts as a front-end processor for the optical field, and the postprocessing algorithms, such as point multiplication and the pseudo-inverse, increase the information extracted from the raw image data. We describe several systems incorporating various features from the categories described in Sec. 2. Experiments are currently underway to demonstrate VHI implementations for 3-D translucent objects using Radon transform approaches. Our future research goals include building resonant holographic imaging systems for surface profilometry and implementing efficient inversion algorithms to obtain real-time data from *N*-ocular VHI systems.

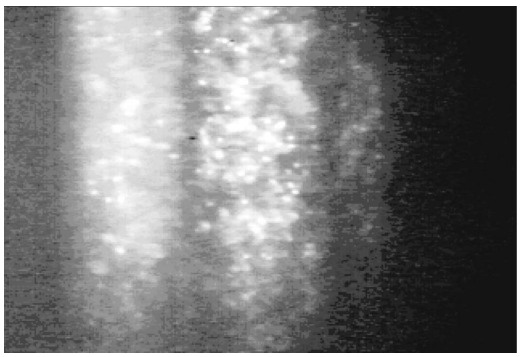

Fig. 20 From Ref. 31, experimental demonstration of real-time hyperspectral microscope. Three holograms were multiplexed within the same volume to look at three different depth layers of a 3-D object that consisted of fluorescent microspheres of diameter 15 μm. The Bragg selectivity of the hologram allows us to simultaneously image three depth slices (one slice is much fainter than the other on account of some recording irregularities); the width of each slice corresponds to the fluorescence bandwidth.

Acknowledgments

We are grateful to Tina Shih, Kehan Tian, Robert Murphey, and Brian H. Miles for helpful discussions. This project was funded by the Air Force Research Laboratories (Eglin Air Force Base) and the Charles Stark Draper Laboratory. George Barbastathis also acknowledges the support of the National Science Foundation through the CAREER (formerly Young Investigator) Award.

References

1. M. V. Klein and T. E. Furtak, *Optics*, Wiley, New York (1986).
2. A. P. Pentland, "A new sense for depth of field," *IEEE Trans. Pattern Anal. Mach. Intell.* **9**, 523–531 (1987).
3. P. Cavanagh, "Reconstructing the third dimension: Interactions between color, texture, motion, binocular disparity and shape," *Comput. Vis. Graph. Image Process.* **37**(2), 171–195 (1987).
4. A. M. Bruckstein, "On shape from shading," *Comput. Vis. Graph. Image Process.* **44**(2), 139–154 (1988).
5. O. Faugeras and Q. T. Luong, *The Geometry of Multiple Images*, MIT Press, Cambridge, MA (2001).
6. M. Minsky, "Microscopy apparatus," U.S. Patent No. 3,013,467 (Dec. 1961).
7. W. H. Carter and E. Wolf, "Correlation theory of wavefields generated by fluctuating, three-dimensional, primary, scalar sources I. General theory," *Opt. Acta* **28**, 227–244 (1981).
8. K. Itoh and Y. Ohtsuka, "Fourier-transform spectral imaging: retrieval of source information from three dimensional spatial coherence," *J. Opt. Soc. Am. A* **3**(1), 94–100 (1986).
9. J. Rosen and A. Yariv, "Three-dimensional imaging of random radiation sources," *Opt. Lett.* **21**(14), 1011–1013 (1996).
10. D. L. Marks, R. A. Stack, D. J. Brady, D. C. Munson, Jr., and R. B. Brady, "Visible cone-beam tomography with a lensless interferometric camera," *Science* **284**(5423), 2164–2166 (1999).
11. D. Huang, E. A. Swanson, C. P. Lin, J. S. Schuman, W. G. Stinson, W. Chang, M. R. Hee, T. Flotte, K. Gregory, C. A. Puliafito, and J. G. Fujimoto, "Optical coherence tomography," *Science* **254**(5035), 1178–1181 (1991).
12. A. V. Jelalian, *Laser Radar Systems*, Artech House, Boston, MA (1992).
13. C. M. Vest, "Formation of images from projections: Radon and abel transforms," *J. Opt. Soc. Am.* **64**(9), 1215–1218 (1974).
14. G. Barbastathis and D. J. Brady, "Multidimensional tomographic imaging using volume holography," *Proc. IEEE* **87**(12), 2098–2120 (1999).
15. P. J. van Heerden, "Theory of optical information storage in solids," *Appl. Opt.* **2**(4), 393–400 (1963).
16. J. W. Goodman, *Introduction to Fourier Optics*, 2nd ed., McGraw-Hill, New York (1996).

17. P. Yeh, *Introduction to Photorefractive Nonlinear Optics*, Wiley & Sons, New York (1993).
18. E. N. Leith, A. Kozma, J. Upatnieks, J. Marks, and N. Massey, ''Holographic data storage in three-dimensional media,'' *Appl. Opt.* **5**(8), 1303–1311 (1966).
19. G. T. Sincerbox, ''Holographic storage—the quest for the ideal material continues,'' *Opt. Mater. (Amsterdam, Neth.)* **4**(2,3), 370–375 (1995).
20. M. P. Bernal, G. W. Burr, H. Coufal, R. K. Grygier, J. A. Hoffnagle, C. M. Jefferson, R. M. McFarlane, R. M. Shelby, G. T. Sincerbox, and G. Wittmann, ''Holographic-data-storage materials,'' *MRS Bull.* **21**(9), 51–60 (1996).
21. G. Barbastathis and D. Psaltis, ''Volume holographic multiplexing methods,'' in *Holographic Data Storage*, H. J. Coufal, D. Psaltis, and G. T. Sincerbox, Eds., Springer Optical Sciences, Berlin (2000).
22. F. H. Mok, G. W. Burr, and D. Psaltis, ''A system metric for holographic memory systems,'' *Opt. Lett.* **21**(12), 896–898 (1996).
23. M. Born and E. Wolf, *Principles of Optics*, 7th ed., Pergamon Press, Cambridge, UK (1998).
24. A. Sinha, W. Sun, T. Shih, and G. Barbastathis, ''Volume holographic imaging in the transmission geometry,'' *Appl. Opt.* **43**(7), 1533–1551 (2004).
25. C. Gu, J. Hong, and S. Campbell, ''2-D shift-invariant volume holographic correlator,'' *Opt. Commun.* **88**(4–6), 309–314 (1992).
26. D. Psaltis and N. Farhat, ''Optical information-processing based on an associative-memory model of neural nets with thresholding and feedback,'' *Opt. Lett.* **10**(2), 98–100 (1985).
27. A. Sinha and G. Barbastathis, ''Volume holographic telescope,'' *Opt. Lett.* **27**, 1690–1692 (2002).
28. A. Sinha and G. Barbastathis, ''Volume holographic imaging for surface metrology at long working distances,'' *Opt. Express* **11**(24), 3202–3209 (2003).
29. J. White, H. Ma, J. Lang, and A. Slocum, ''An instrument to control parallel plate separation for nanoscale flow control,'' *Rev. Sci. Instrum.* **74**(11), 4869–4875 (2003).
30. A. Sinha, W. Sun, T. Shih, and G. Barbastathis, ''*N*-ocular holographic 3d imaging,'' In OSA Annual Meeting, Orlando, FL, 2002, paper WD7.
31. W. Liu, D. Psaltis, and G. Barbastathis, ''Real time spectral imaging in three spatial dimensions,'' *Opt. Lett.* **27**, 854–856 (2002).
32. A. Sinha, W. Sun, and G. Barbastathis, ''Broadband volume holographic imaging,'' Appl. Opt. (in press).
33. A. Sinha, W. Sun, and G. Barbastathis, ''*N*-ocular volume holographic imaging,'' Appl. Opt. (in press).
34. G. Barbastathis and A. Sinha, ''Information content of volume holographic imaging,'' *Trends Biotechnol.* **19**(10), 383–392 (2001).